

End-to-End Deep Learning of Lane Detection and Path Prediction for Real-Time Autonomous Driving

Der-Hau Lee and Jinn-Liang Liu

Abstract—We propose an end-to-end three-task convolutional neural network (3TCNN) having two regression branches of bounding boxes and Hu moments and one classification branch of object masks for lane detection and road recognition. The Hu-moment regressor performs lane localization and road guidance using local and global Hu moments of segmented lane objects, respectively. Based on 3TCNN, we then propose lateral offset and path prediction (PP) algorithms to form an integrated model (3TCNN-PP) that can predict driving path with dynamic estimation of lane centerline and path curvature for real-time autonomous driving. We also develop a CNN-PP simulator that can be used to train a CNN by real or artificial traffic images, test it by artificial images, quantify its dynamic errors, and visualize its qualitative performance. Simulation results show that 3TCNN-PP is comparable to related CNNs and better than a previous CNN-PP, respectively. The code, annotated data, and simulation videos of this work can be found on our website for further research on NN-PP algorithms of autonomous driving.

Index Terms—Deep learning, convolutional neural network, lane detection, path prediction, autonomous driving.

I. INTRODUCTION

Lane detection is an essential task of advanced driver assistance systems (ADAS) in modern vehicles and autonomous driving systems in self-driving cars for lane keeping assistance, departure warning, and centering [1], [2], [3], [4], [5], [6], [7]. There are two major paradigms, namely, classic computer vision and deep learning, for lane detection [1]. The classic computer vision paradigm requires intensive feature engineering, road modeling, and special case handling and is thus not robust enough to deal with seemingly infinite driving situations, environments, and unexpected obstacles [1]. The deep learning paradigm has recently shown considerable progress to alleviate these difficulties [1], [2], [3], [4], [5], [6], [7].

Path prediction (lane following) is also a crucial task of ADAS and self-driving vehicles for active driving assistance and lateral and longitudinal controls [5], [8]. It depends on various factors of vehicles and road and traffic environment such as ego vehicle's speed and steering angle, road geometry, and the other closest in-path vehicle [5], [8]. It also involves perception, sensory, and control systems in the ego vehicle [8].

We propose an end-to-end three-task convolutional neural network (3TCNN) that performs two regression tasks

of bounding boxes [1], [2] and Hu moments [9] and one classification task of object masks [1], [2] for lane detection and road recognition. Based on 3TCNN, we also propose lateral offset and path prediction (PP) algorithms to form an integrated model (3TCNN-PP) that can predict driving path with dynamic estimation of lane centerline and path curvature for real-time autonomous driving. The related work and our contribution are briefly described as follows.

A. Related work

Sermanet et al. proposed OverFeat [10] for detecting objects in images using a sliding window approach. OverFeat comprises a feature extractor by AlexNet (truncated without fully connected layers) [10], a multi-scale (on image resolution) classifier by a sliding window detector on feature maps to produce 3D output maps (two spatial dimensions and a classification vector), and a box regressor for accumulating rather than suppressing bounding boxes of objects to increase detection confidence. It is the winner of the localization task of the ImageNet Large Scale Visual Recognition Challenge in 2013.

Huval et al. proposed OverFeat-Mask [1] by adding a mask detector to the sliding window of OverFeat for reducing false positives of predicting cars and the computational complexity of the bounding box merging algorithm for real-time lane and car detection. The mask detector produces object masks yielding much fewer bounding boxes so that the box regressor can avoid choosing two valid objects in its context view. Unlike vehicles having blob shapes, long lane lines or curves cannot fit into single bounding boxes. The lane regressor predicts two endpoints of a local line segment and their depth (six dimensions) with respect to a monocular camera. The box regressor predicts the coordinates and the depth (five dimensions) of the bounding boxes of line segments.

Lee et al. proposed VPGNet [2] for lane and road marking detection and recognition and for vanish point (VP) prediction to guide (G) lane lines under adverse weather conditions. VPGNet consists of a shared feature extractor (truncated AlexNet), a box regressor for road markings (crosswalks, stop lines, speed bumps, arrows etc.), a grid-level mask detector (classifier) for detecting thin lines by projecting pixel-level annotations to grid-level masks, a multi-label classifier for various lane and road marking classes, and a vanish point predictor (classifier), a total of four sub-networks branching from the feature extractor.

Hu moments are classic tools in a wide range of computer vision and image analysis applications for feature extraction

This work was supported by the Ministry of Science and Technology, Taiwan, under Grant MOST 109-2115-M-007-011-MY2.

D. Lee was with the Department of Electrophysics, National Chiao Tung University, Hsinchu 300, Taiwan.

J. Liu is with the Institute of Computational and Modeling Science, National Tsing Hua University, Hsinchu 300, Taiwan (e-mail: jinliu@mail.nd.nthu.edu.tw, website: <http://www.nhcue.edu.tw/~jinliu>).

and pattern recognition [9]. However, they have not yet been used for lane detection and road recognition in the deep learning paradigm to our knowledge. They are weighted averages of pixel intensities in images and invariant to the size, position, and orientation of image objects in continuous domains [9]. We find that the first two Hu moments can be used to construct a CNN model that can perform lane detection for localization and global road recognition for path prediction similar to the vanish point prediction to guide lane lines in VPGNet.

Path prediction models are generally polynomials of lane centerline having few coefficients determined by heading and lane curvature without [5] or with considering vehicle's transient dynamics such as yaw rate and lateral and longitudinal velocities [8]. Cudrano et al. [5] proposed an integrated NN-PP model that uses vehicle's heading and lateral displacement calculated from the lane detection output of a modified U-Net to determine a cubic polynomial. They validated their model in a real car driving on two racetracks (one is more curvy and the other is less) without other cars and with a maximum speed of 54 km/h. They detailed their PP algorithm with validation results but did not present the overall architecture of their NN-PP model and the details of the modified U-Net and its performance on lane detection.

We proposed a deep learning model in [11] that combines multi-task CNN and control algorithms for multiple actions in autonomous driving (steering, acceleration, braking, lane changing, and overtaking). We also modified The Open Racing Car Simulator (TORCS) implementing the model for a host car (Host) efficiently inferring and stably driving with other autonomous cars (Agents) in dynamic TORCS traffic. We extend here our TORCS to include lane detection and path prediction in order to test and evaluate the overall performance of deep learning, lane detection, and path prediction algorithms in the simulator before deploying them to real cars in real world traffic.

B. Contribution

Little work exists on the architecture of deep learning models and path prediction algorithms for self-driving cars to perform lane detection, road recognition, and lane following in dynamic traffic [5], let alone the overall performance of these algorithms. We propose such an architecture and present its pipeline modules and performance details. We show that Hu moments in classic computer vision can be used in the deep learning paradigm for both lane localization and global road guidance. We also develop and provide a modified TORCS software for further research and development of lane detection and path prediction which are critical in advanced driver assistance or autonomous driving systems.

II. END-TO-END DEEP LEARNING OF LANE DETECTION AND PATH PREDICTION

Fig. 1 illustrates the architecture of our deep learning and path prediction algorithms implemented in TORCS from Host's view with several Agents in dynamic traffic. The architecture consists of (a) images from Host's front-facing camera, (b) gray lane images obtained from 3TCNN and their

region of interest (RoI) for lane localization and centering, (c) a perspective mapping (PM) of lane lines and their clustering from camera's view (CV) to top-down view (TDV) for path prediction and curvature estimation, and (d) the inverse PM transforming TDV back to CV lines in the original image with lane line (blue) fitting and driving path (green) prediction and lateral offset estimation. More details about these four sub-figures and corresponding methods are given below.

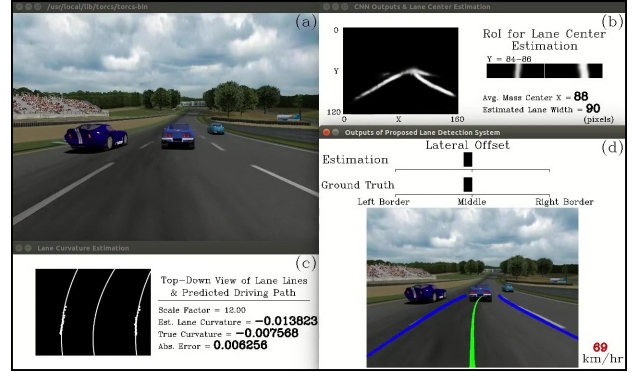


Fig. 1. A real-time simulation architecture of lane detection and path prediction by 3TCNN-PP from a host car's view in TORCS traffic: (a) input image, (b) lane detection, (c) line clustering and perspective transformation, and (d) lateral offset estimation, inverse perspective transformation, line (blue) fitting, and driving path (green) prediction.

A. 3TCNN model of lane detection

3TCNN consists of a feature extractor of five convolutional layers shared by a box regressor for localizing lane lines, a mask detector for classifying line objects and their background, and a regressor of Hu moments for recognizing road and lane patterns (three branches for three tasks) as shown in Fig. 2 with the dimensions of all layers. Each branch has three convolutional layers and one output layer. The extractor, the box regressor, and the object mask detector are similar to those in [1], [2], [10].

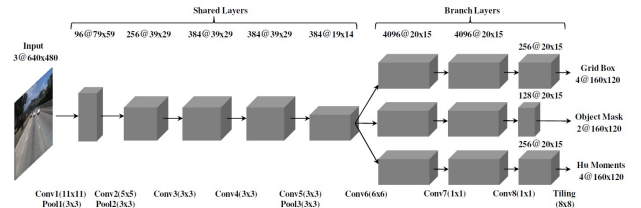


Fig. 2. Three-task CNN (3TCNN) consists of a feature extractor shared by a box regressor, a mask detector, and a regressor of Hu moments performing localization, classification, and recognition tasks, respectively.

In addition to the four coordinates $(x_{\min}^k, y_{\min}^k, x_{\max}^k, y_{\max}^k)$ of each one (k) of all grid (bounding) boxes of lane markings for $k = 1, 2, \dots$ [1], [2], we propose to use $(h_1^{0,k}, h_2^{0,k}, h_1^{m,k}, h_2^{m,k})$ as four additional labels for recognizing road (global) and lane (local) patterns in an traffic image as shown in Fig. 3a. Here, $h_1 = \eta_{20} + \eta_{02}$ and $h_2 = (\eta_{20} - \eta_{02})^2 + 4\eta_{11}^2$ are first and second Hu moments [9], respectively, $\eta_{pq} = \mu_{pq} / \mu_{00}^{1+(p+q)/2}$ and $\mu_{pq} = \sum_x \sum_y (x -$

$\bar{x}^p(y-\bar{y})^q I(x,y)$ are normalized central and central moments with non-negative integers p and q such that $p+q \leq 2$, $I(x,y) = 0$ or 1 is the pixel intensity of a binary image in black and white at pixel coordinates (x,y) as shown in Fig. 3b (an annotated ground-truth image from TuSimple dataset [3], [6]), and $(\bar{x}, \bar{y}) = (\frac{\mu_{10}}{\mu_{00}}, \frac{\mu_{01}}{\mu_{00}})$ is the image's centroid.

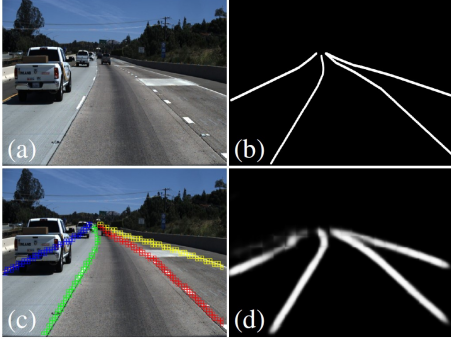


Fig. 3. (a) A TuSimple image [3], [6]. (b) Binary (ground truth) image of four lane lines of (a) in black and white. (c) Ground truth bounding boxes (8x8 in pixel size) of four lines in colors. (d) Predicted lane lines of (a) by 3TCNN in grayscale.

The labels $h_1^{0,k}$ and $h_2^{0,k}$ are moments calculated from the entire (global) binary image of the road in contrast to four sets of moments $h_1^{m,k}$ and $h_2^{m,k}$ from four separate (local) lines of Host's lane and two adjacent lanes for $m = 1, 2, 3, 4$ from left ($m = 1$) to right ($m = 4$) as shown in Fig. 3c by color boxes. The moments $X = h_1$ and $Y = \sqrt{h_2}$ characterize the 'spread' and 'slenderness' of an object, respectively. The point (X, Y) in 2D space can thus capture the pattern of the object [9]. We find that these two second-order moments of seven Hu moments are dominant and sufficient for lane detection and road recognition. These labels are used to train the sub-network of Hu moments with the other two sub-networks for detecting lane lines and recognizing road pattern that includes the vanishing area as shown in Fig. 3d which is an output road image of 3TCNN in normalized grayscale with $0 \leq I(x,y) \leq 1$.

3TCNN thus extends 2TCNN, the 2-task (grid box and object mask) CNN, to include the Hu-moment regressor replacing the vanish point prediction task in [2] for lane localization as well as global geometric-context recognition of roads under adverse conditions [2]. The object mask task uses softmax loss, while grid box and Hu-moment tasks use L1-loss [2] for CNN optimization.

B. Lateral offset estimation

Cameras mounted on vehicles vary in height and lateral location so do lane images [7]. We choose the region of interest (RoI shown in Fig. 1b) of output gray images (160x120 output probability maps in pixel size) in the range of $y = 84 \sim 86$ for lane centering by calculating the centroid coordinate \bar{x} . The coordinates of left ($x = 0 \sim 80$) and right ($x = 81 \sim 159$) parts of gray images are \bar{x}_l and \bar{x}_r calculated separately. The lane center is estimated as $(\bar{x}_l + \bar{x}_r)/2$ and the lane width is $\bar{x}_r - \bar{x}_l$. Since the image center is at $x = 80$, the distance from

Host to the lane center is estimated by $\Delta_0 = 80 - (\bar{x}_l + \bar{x}_r)/2$. However, this approach tends to overestimate the true distance to the lane center since RoI is ahead of Host and depends on camera's position. We use $\Delta = \alpha\Delta_0$ with $\alpha = 0.6$ as an estimated offset to the true lane center shown in Fig. 1d. This lane centering is thus a CNN-based method.

C. Driving path prediction

The following path prediction algorithm comprises well-known or advanced post-processing methods that are particularly suitable for output images having Hu-moment local and global properties to deal with complexity, scalability, and homography issues [3], [6], [7].

Path Prediction Algorithm:

Step 1. We use Otsu's binarization method and morphological erosion [12] to remove isolated (noisy) points in gray images and DBSCAN [1] to cluster detected line segments (dots in Fig. 1c).

Step 2. A perspective mapping [2], [6], [7] then transforms semantic lanes from camera's view to top-down view space to which quadratic polynomials [4] apply for fitting parallel lane lines (Fig. 1c) by using recursive least squares [5] and imposing parallelism.

Step 3. Another quadratic polynomial $f(x)$ for the desired driving path is uniquely determined by three conditions, i.e., the starting (x_s) and final (x_f) points of the middle line (Fig. 1c) of two parallel lines and its tangent at x_s as that of the parallel lines. We thus obtain the TDV lane curvature $\kappa_0 = f''(x_s)/[1 + f'(x_s)]^{3/2}$ at x_s in 1/m unit. The true curvature $\kappa = \beta\kappa_0$ in the real world space with a scale factor $\beta = 12$ is then used to calculate its error compared to the ground truth curvature of TORCS track as shown in Fig. 1c.

Step 4. Finally, the inverse PM transforms these three lines back to the CV space for visual verification and lateral estimation shown in Fig. 1d.

In Step 1, we use five consecutive gray images to obtain averaged line segments for possible occluded or worn-out markings. Higher-order polynomials and corresponding PM transformations are generally needed in Steps 2 and 3 for curvy or up-and-down roads in real world [3], [7].

III. EXPERIMENTAL SETUP

A. Ground truth values and performance measures

The ground truth values of the grid (bounding) box (GB), object mask (OM), and Hu moments in the three output layers of Fig. 2 are defined as follows. These layers consist of a grid of 160x120 cells. Each cell represents 4x4 pixels in the original 640x480 resolution of input images. If a cell has lane-marking pixels, its binary value is 1 (a part of an OM) else is 0 for the OM classification task. Each ground truth GB is an OM consisting of 2x2 cells and its normalized coordinates and Hu moments are ground truth values for the GB and Hu regression tasks, respectively.

The lane detection results of a CNN are paired up with ground truth values into four cases, namely, true positive, true negative, false positive, and false negative. Its performance is measured in accuracy, precision, recall, and F1 score [1],

[2], [3]. To determine these scores, CNN’s output probability maps are first resized to that of original images. The minimum distance R of each pixel in the resized map from ground truth GBs is then computed [2]. The true or false value of that pixel is defined as the average outcome from two cases $R \leq 10$ and $R \leq 20$.

B. Data

We use TuSimple (real world) images [3], [6] (as in Fig. 3a) to train and test our 2T/3TCNN for lane detection. We then use TORCS (artificial) images (Fig. 1a) to evaluate the overall performance (Figs. 1b-1d) of the integrated model of the trained 3TCNN and path prediction algorithms from Host’s perspective in real-time and dynamic traffic with other Agents.

The TuSimple set consists of 3626 training and 2782 testing images recorded on countryside and highway roads with 2-5 lanes in daytime. To enlarge training data, we use 6294 and 114 images in training and testing phases, respectively. The data set contains binary images of all lane lines as well. In training phase, we extract individual lane lines as new binary images containing single lines and then calculate local Hu moments $(h_1^{m,k}, h_2^{m,k})$ of each image with $m = 1$ to 4 for four lane lines and $k = 1, \dots$, for all grid boxes of lane markings. Similarly, all-line images yield global $(h_1^{0,k}, h_2^{0,k})$. Traffic, all-line, and single-line images with ground-truth coordinates and Hu moments of GBs are all inputs to CNNs for training and testing.

We train 2TCNN (as in [2]) and 3TCNN on TuSimple images by stochastic gradient descent with a batch size of 25, the momentum 0.9, and the learning rate starting from 0.01 and decreasing by a factor of 0.1 every 100k iterations. Both CNNs converge rapidly as shown in [2] since the lane marking area of the images used for training is much smaller than the background area. 3TCNN is better than 2TCNN because its additional task of Hu moments has positive correlation effects on the other two (grid box and object mask) tasks yielding better gradients in minimizing training loss and thus more activated neurons for inferring lane boundaries. The more tasks a model has, the better convergence it is but with larger complexity as also shown in [2].

We evaluate the dynamic performance (as shown in Fig. 1) of the integrated 3TCNN-PP model in TORCS for Host driving with 6 Agents and lane changes on two different tracks shown in Fig. 4, where Track A (left) and Track B (right) are less and more curvy three-lane roads, respectively. Each lane width is 4 m. The total lengths of Tracks A and B are 3919 and 4441 m, respectively. All cars drive autonomously by default algorithms of TORCS [11] with the maximum speed of 70 and 67 km/h for Host (displayed in Fig. 1d) and Agents, respectively. The ground-truth TORCS data include 3200 images from each track collected by Host driving along the middle lane for more than one lap without other Agents for calculating static and dynamic errors [11] of curvature and lateral offset by 3TCNN-PP.

IV. RESULTS

Table I shows the performance of 2TCNN and 3TCNN for lane detection on TuSimple testing data. Accuracy and

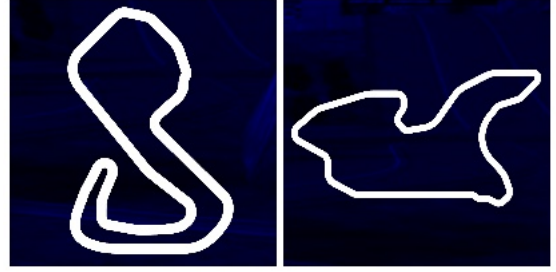


Fig. 4. TORCS Tracks A (left) and B (right) are less and more curvy three-lane roads, respectively.

TABLE I
PERFORMANCE OF 2T/3TCNN

Accuracy	Recall	F1 score	Precision
0.943/0.946	0.867/0.868	0.833/0.839	0.801/0.811

F1 score results agree with those in [2] and [3] using grid-wise and pixel-wise measures, respectively. 3TCNN is slightly better than 2TCNN in F1 score also shown in [2]. Refs. [2], [3] do not have Precision and Recall results for lane detection task.

Table II shows the overall performance of 3TCNN-PP (integrating 3TCNN and path prediction algorithms) in real-time simulations on Tracks A and B. The performance is measured in the static and dynamic mean absolute errors (sMAE/dMAE) [11] in predicting the curvature κ (in 1/m) and lane center distance Δ (m) of the path traversed by Host in TORCS traffic with other Agents. Here, dMAE is larger than sMAE due to asynchronous frequencies between 3TCNN-PP computing (complexity, computer, and speed dependent) and TORCS image generation (computer and speed dependent) [11]. 3TCNN-PP and TORCS frequencies are > 20 and > 30 Hz on our computer, respectively, comparable to that of [7]. Table II also presents the corresponding percentage (%) of available frames (Avail) [5] in Host’s videos for prediction, which is less than 100 due to shadows or occlusions on the road and is worse in dynamic than in static conditions.

The dMAE of lateral offset Δ is smaller (better) than sMAE showing that the lateral offset algorithm performs better lateral corrections for Δ in dynamic motion than in stationary. Table II thus also shows the importance of lateral offset estimation from car’s camera images for path planning in autonomous driving. Our model performs better than that of [5] (cf. Table

TABLE II
PERFORMANCE OF 3TCNN-PP IN STATIC AND DYNAMIC ERRORS (sMAE/dMAE) WITH THE PERCENTAGE (%) OF AVAILABLE FRAMES (AVAIL) ON TRACKS A AND B

	Track A	Track B
	sMAE/dMAE	
κ (1/m)	0.0086/0.0086	0.0103/0.0105
Δ (m)	0.0531/0.0489	0.0539/0.0525
	Avail (%)	
κ	99.59/99.64	100/99.97
Δ	92.26/91.56	82.4/81.30

I) in an order of magnitude (94.6 vs. 5.39 cm in the worst Δ on different (real-world vs. artificial) roads by different (real vs. artificial) cars). Cudrano et al. [5] modified CNN U-net and integrated it in a perception pipeline that includes Δ calculations but without using learning methods for lateral corrections like our lateral offset estimation.

Fig. 5 illustrates the ground-truth (black) and estimated (blue dotted) curves of κ and Δ in sMAE with respect to the frame number of the videos from Tracks A and B on which Host drives alone in the middle lane, where each point of the curves is an average of 11 values of κ or Δ from consecutive frames. The κ and Δ curves are reciprocal in peaks and valleys as in their units. The curvature κ curve is relatively more noisy due to more errors incurred in calculating $f'(x_s)$ and $f''(x_s)$ in the curvature κ_0 formula. Two videos are available on our website for a qualitative and quantitative review on the dynamic performance of 3TCNN-PP from Host driving on these two tracks with other Agents and lane changes in real time simulation.

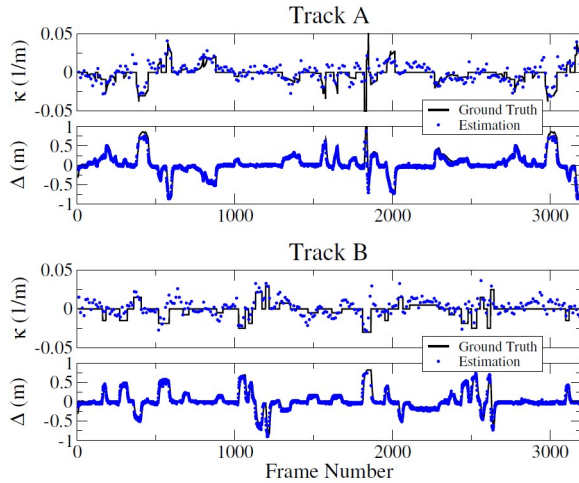


Fig. 5. Estimated (blue) and ground-truth (black) curvatures (κ) and distances to lane center (Δ) on Tracks A and B.

V. CONCLUSION

We propose a three-task CNN (3TCNN) that comprises bounding-box and Hu-moment regressors and object-mask classifier for lane detection and road recognition. It is based on the local and global properties of lane lines and road structure using the first and second Hu moments of camera images. We also propose a model to integrate both lane detection and path prediction (PP) algorithms and develop a simulator to evaluate the dynamic performance of the model qualitatively as well as quantitatively from a host car driving with other cars and lane changes. We give a detailed description of the simulation architecture from input images to the projective mapping and error estimation of 3TCNN-PP results. 3TCNN and 3TCNN-PP results are comparable to those of related CNNs and better than a previous NN-PP by an order of magnitude, respectively.

REFERENCES

[1] B. Huval, et al., "An empirical evaluation of deep learning on highway driving," *arXiv:1504.01716*, 2015.

[2] S. Lee, et al., "VPGNet: Vanishing point guided network for lane and road marking detection and recognition," in *Proceedings of the IEEE International Conference on Computer Vision*, pp. 1947-1955, 2017.

[3] D. Neven, et al., "Towards end-to-end lane detection: an instance segmentation approach," in *IEEE Intelligent Vehicles Symposium (IV)*, pp. 286-291, 2018.

[4] N. Garnett, et al., "3D-LaneNet: End-to-end 3D multiple lane detection," in *Proceedings of the IEEE International Conference on Computer Vision*, pp. 2921-2930, 2019.

[5] P. Cudrano, et al., "Advances in centerline estimation for autonomous lateral control," in *IEEE Intelligent Vehicles Symposium (IV)*, pp. 1415-1422, 2020.

[6] X. Li, J. Li, X. Hu, and J. Yang, "Line-CNN: End-to-End traffic line detection with line proposal unit," *IEEE Transactions on Intelligent Transportation Systems*, vol. 21, pp. 248-258, 2020.

[7] P. Lu, et al., "SUPER: A novel lane detection system," *arXiv:2005.07277*, 2020.

[8] C. F. Lin, A. G. Ulsoy, and D. J. LeBlanc, "Vehicle dynamics and external disturbance estimation for vehicle path prediction," *IEEE Transactions on Control Systems Technology*, vol. 8, pp. 508-518, 2000; W., Kim, et al., "Vehicle path prediction using yaw acceleration for adaptive cruise control," *IEEE Transactions on Intelligent Transportation Systems*, vol. 19, pp. 3818-3829, 2018.

[9] M. K. Hu, "Visual pattern recognition by moment invariants," *IRE Transactions on Information Theory*, vol. 8, pp. 179-187, 1962; S. O. Belkassim, M. Shridhar, and M. Ahmadi, "Pattern recognition with moment invariants: a comparative study and new results," *Pattern Recognition*, vol. 24, pp. 1117-1138, 1991.

[10] P. Sermanet, et al., "Overfeat: Integrated recognition, localization and detection using convolutional networks," *arXiv:1312.6229*, 2013.

[11] D.-H. Lee, et al., "Deep learning and control algorithms of direct perception for autonomous driving," *Applied Intelligence*, vol. 51, pp. 237-247, 2021.

[12] R. F. Moghaddam and M. Cheriet, "AdOtsu: An adaptive and parameter-less generalization of Otsu's method for document image binarization," *Pattern Recognition*, vol. 45, pp. 2419-2431, 2012.